Strong Metal Support Interaction in Ru/V_2O_3 Mitigates Reactant Induced Poisoning in Succinic Acid Hydrogenation

Yayati Naresh Palai,[a] Eti Mahal,[b] Biswarup Pathak,* [b] Atsushi Fukuoka,* [a] and Abhijit Shrotri*[a]

[a] Dr. Y.N. Palai, Prof. Dr. A. Fukuoka, Dr. A. Shrotri
Institute for catalysis, Hokkaido University
Sapporo Hokkaido, Japan, 001-0021
E-mail: ashrotri@cat.hokudai.ac.jp, fukuoka@cat.hokudai.ac.jp

[b] Eti Mahal, Prof. Dr. B. Pathak
Department of Chemistry, Indian Institute of Technology (IIT) Indore
Indore, Madhya Pradesh, India, 453552
E-mail: biswarup@iiti.ac.in

Supporting information for this article is given via a link at the end of the document.

Abstract: Hydrogenation of carboxylic acids to lactones is an important reaction. However, strong adsorption of carboxylic acid on the catalyst causes poisoning of the active site and demands harsher reaction condition and organic solvents. In this study, we demonstrate that strong metal support interaction (SMSI) and hydrogen spillover on Ru/V_2O_3 can counter such poisoning effect. The catalyst with SMSI was able to hydrogenate succinic acid to γ-butyrolactone (GBL) in 77% yield in the presence of water at mild conditions of 150 °C. H_2-D_2 exchange experiment showed that for Ru/V_2O_3 catalysts reduced at higher temperatures SMSI created a barrier between the substrate and the hydrogen dissociation sites. Moreover, the spillover of dissociated H_2 onto the V_2O_3 surface was found to enhance catalytic activity. Thermodynamic calculations using density functional theory showed that transfer of a hydride from Ru and proton from V_2O_3 to the substrate have a lower reaction free energy compared to the transfer of two hydrogen atoms from the ruthenium surface. Additionally, the easier desorption of product from the Ru/V_2O_3 surface increased catalytic activity. We show that SMSI can be used as an effective strategy to mitigate the poisoning of metal sites during catalytic hydrogenation of carboxylic acids.

Introduction

Hydrogenation of carboxylic acids to alcohols and lactones is an important reaction in biomass chemistry. In particular, biobased diacids like succinic acid serve as key renewable feedstocks for producing valuable chemicals. These include γ-butyrolactone (GBL) [1–6], 1,4-butanediol (BDO) [7,8], and tetrahydrofuran (THF) [9–13], which are used for polymer production, pharmaceuticals, and solvent synthesis as alternatives to petroleum-derived products[14]. Among these, GBL, obtained via catalytic hydrogenation of succinic acid (**Figure 1**), is particularly attractive due to its role as a versatile intermediate in biobased chemical production [15–18].

Supported noble metal catalysts, including Pt, Pd, Rh, and Ru, have been widely studied for the hydrogenation of succinic acid to GBL, typically at high temperatures (~240 °C) and high H_2 pressures (6 MPa or higher) in 1,4-dioxane as a solvent [1–6]. While several of these studies report promising yields of GBL, the requirement for harsh reaction conditions and organic solvents limits their practical application. Therefore, there is a need to design catalysts that enable the hydrogenation of succinic acid under milder conditions in aqueous media to improve process sustainability and reduce the carbon footprint.

Several catalytic design strategies have been explored to improve performance, including the use of oxophilic metals to enhance the adsorption of intermediates [8,9], size reduction of metal particles to enhance atom utilization efficiency [4], and tuning the acidity/basicity of supports [5]. However, reports on identifying the sites for adsorption of carboxylic acids and their influence on catalytic activity are less studied. Carboxylic acids are known to strongly adsorb on metal surfaces, which poisons the active sites and reduces activity at mild conditions [19–22]. Yakabi et al. reported that a strong bidentate adsorption of succinic acid over Ru lowers the selectivity of GBL due to decarboxylation, while monodentate adsorption on Pd showed higher selectivity for GBL [3]. Primo et al. reported that activity for the hydrogenation of carboxylic acid can be increased using a Ru/TiO_2 where the carboxylic acid was weakly bound to the support near smaller metal nanoparticles, which provide H_2 for the hydrogenation reaction. In contrast, strongly bound carboxylic acid on Ru/CeO_2 was difficult to hydrogenate due to poisoning [23]. Additionally, strong coordination of dicarboxylic acids with metal atoms of the catalyst also causes deactivation by leaching [19,20]. Therefore, limiting the strong adsorption of dicarboxylic acids on the metal surface should mitigate the poisoning of the active site and increase activity at mild conditions.

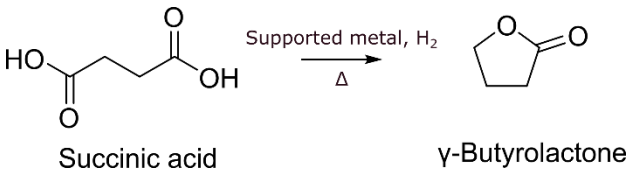

Figure 1. Scheme showing succinic acid hydrogenation to GBL.

In this study, we show that by covering metal nanoparticles with oxide an phase in Ru/V_2O_3 through strong metal support interaction (SMSI) [24–26], the substrate-induced poisoning can be reduced by isolation of Ru sites from succinic acid. H_2 dissociation at the interface of Ru and V_2O_3 is enhanced in catalysts with SMSI. Furthermore, the spillover of dissociated H_2 over the partially reduced V_2O_3 surface led to the hydrogenation of succinic acid adsorbed on the support to GBL under mild reaction conditions in the presence of water. This approach enables efficient GBL production under mild reaction conditions in the presence of water, providing a pathway toward more sustainable catalytic processes.

Experimental

Catalyst synthesis

All the catalysts were prepared via the wet impregnation method. In a typical synthesis, 500 mg of commercial V_2O_3 support (TCI Chemicals) was dispersed in 20 mL of water, followed by addition of an aqueous solution of $Ru(NO)(NO_3)_3$ to achieve desired Ru loading. The solution was evaporated at 40 °C at 60 mbar pressure, then the catalyst was dried and reduced at different temperatures for 1 h under 30 mL min^{-1} H_2 flow. The catalysts were named Ru/V_2O_3-X, where X was the reduction temperature. Catalysts using other supports were also prepared using the same method unless specified otherwise and were reduced at 400 °C. The heating rate during reduction was set at 10 °C min^{-1} for all catalysts.

Catalyst Characterizations

X-ray diffraction (XRD) patterns were recorded with a Rigaku Ultima IV using a Cu Kα X-ray source (λ = 1.54 Å) operating at 40 kV and 20 mA with powdered samples. Scanning transmission electron microscopy (STEM) images were obtained in a JEOL JEM-ARM200F atomic resolution electron microscope. High resolution transmission electron microscopy (HR-TEM) images were taken on a JEOL JEM-2100F microscope. X-ray photoelectron spectroscopy (XPS) was performed with JEOL JPS-9010MC instrument with Mg anode. The spectra were charge corrected by adjusting the adventitious carbon peak to 284.6 eV. In situ Fourier transform infrared (FTIR) spectroscopy was carried out in Perkin Elmer Spectrum 100 IR instrument with a transmission cell (Schematic illustration in **Figure S1**) and triglycerin sulphate (TGS) detector.

Succinic acid hydrogenation

Succinic acid hydrogenation was performed in a 10 mL stainless steel autoclave reactor equipped with a Teflon liner. In a typical reaction, 1 mmol of succinic acid and 50 mg of catalyst was added to 5 mL water. The reactor was closed and filled with 5 MPa of H_2 gas and placed in an oil bath preheated to 150 °C and was stirred through the entire course of reaction.

After the reaction, the reactor was cooled to room temperature and pressure was released. The recovered reaction mixture was centrifuged to separate the product mixture, which was analyzed with an HPLC equipped with an Aminex HPX 87H column and a RID detector with 0.5 mL/min flow of 5 mM H_2SO_4 solution at 50 °C. Succinic acid conversion (χ_t) and product yield (Y_p^t) at time, t was calculated using following equations –

$$\chi_t = \frac{n_r^0 - n_r^t}{n_r^0}$$

$$Y_p^t = \frac{n_p^t}{n_r^0}$$

Where n_r^0 and n_r^t are number of moles of reactant at time 0 and time t respectively and n_p^t is number of moles of product at time t.

Density functional theory calculation

Theoretical calculations were performed with the help of Vienna *Ab initio* Simulation Package (VASP) [27,28]. The projected augmented wave method was implemented to describe the electron-core interactions with a plane wave basis set energy cutoff of 470 eV [29,30]. We have used the generalized gradient approximation as formulated in Perdew−Burke−Ernzerhof (GGA-PBE) functional to consider the exchange and correlation interaction [31]. DFT-D3 dispersion correction as implemented by Grimme was used [32]. During geometry relaxation, convergence criteria for the Force and electronic energy minimization was set to < 0.02 eV $Å^{-1}$ and < 10^{-4} eV, respectively. We have utilized DFT+U approach proposed by Dudarev with U= 1.7 eV for V_2O_3, where the U value was chosen based on the previous theoretical studies on similar systems [33–35]. All the calculations performed were spin polarized. Ru (001) slab was modelled with a (6×6) super cell having 4 layers. To design the Ru/ V_2O_3 catalyst surface with SMSI, we have deposited one V_2O_3 (001) monolayer on top layer of the modelled Ru (001) slab as it is found to be the most stable surface of V_2O_3 in the previous studies [36]. A Γ-centered k-point mesh of 3×3×1 was used to sample the Brillouin zone. All the calculations were performed in gas phase. To avoid periodic interactions a vacuum of ~ 15 Å was added along the z-direction. The reaction free energy changes (ΔG) have been calculated using the following equation,

$$\Delta G = \Delta E + \Delta ZPE - T\Delta S$$

where ΔE is the total energy difference between initial and final states, ΔZPE is the change in zero-point energy. T and ΔS denotes temperature and change in entropy for the reaction, respectively. Usually, the translational and rotational entropies are negligible for the intermediates adsorbed on solid catalyst surfaces. Whereas, vibrational entropy is calculated using the following statistical thermodynamic equation,

$$S_V = R\sum\left(\frac{\hbar\nu_i}{k_BT\left(exp\left(\frac{\hbar\nu_i}{k_BT}-1\right)\right)} - \ln\left(1 - xp\left(-\frac{\hbar\nu_i}{k_BT}\right)\right)\right)$$

Where, S_V denotes the vibrational entropy, R denotes the gas constant, k_B is the Boltzmann constant, T is the temperature, and $\hbar$ = h/2π.

The 300 K temperature has been considered for the entropy correction and zero-point energy can be calculated considering the following equation,

$$ZPE = \sum_i {}^1/_2\, h\nu_i$$

Where ν_i and h are the vibrational frequencies and Planck's constant, respectively.

Results and Discussion

Characterization of Ru/V_2O_3 catalysts

Supported Ru/V_2O_3 catalysts were prepared for succinic acid hydrogenation by impregnation with a Ru loading of 2 wt. %, which was optimized based on catalytic activity (**Figure S2**). This loading was fixed to minimize the influence of metal loading on catalytic performance and ensure a consistent evaluation of the SMSI effect. The catalysts were reduced at different temperatures to achieve varying degrees of SMSI. **Figure 2** shows XRD profiles of the Ru/V_2O_3 catalysts prepared by reducing $Ru(NO)(NO_3)_3$ impregnated V_2O_3 catalysts between 200–500 °C. All the catalysts showed peaks corresponding to V_2O_3 phase and no other phases of vanadium oxide were detected. The crystallite size of V_2O_3 was about 50 nm and did not change with the increase in reduction temperature. Ru crystallite size was beyond the detection limit of

XRD as peaks corresponding to Ru nanoparticles were not observed in XRD pattern.

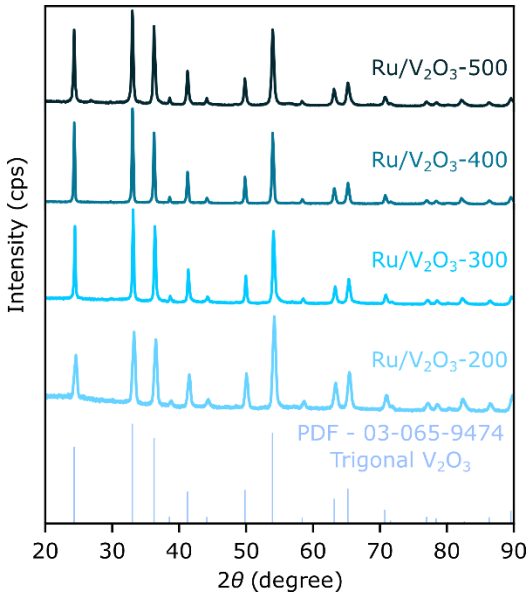

Figure 2. XRD of Ru/V_2O_3 catalysts reduced at different temperatures along with standard trigonal V_2O_3 from PDF2 database.

Figure 3a-h shows STEM images and the corresponding particle size distribution of the Ru/V_2O_3 catalysts. Ru particles were well distributed on the V_2O_3 surface with a narrow size distribution. The average particle size did not change drastically with increase in temperature, and most particles were less than 2 nm in size. However, Ru/V_2O_3-500 exhibited a wider Ru size distribution with an average particle size of 2.8 nm. The surface area of catalysts, calculated from N_2 adsorption isotherms, was low and varied marginally between 5.6–4.7 m^2g^{-1} (**Figure S3**, **Table S1**). The low average particle size of Ru despite the low surface area and high reduction temperature indicated that the temperature dependent aggregation of Ru nanoparticles was limited.

Catalysts reduced at higher temperatures showed a pronounced amorphous phase around the particles, which suggests migration of V_2O_3 support over the surface of metal nanoparticles during thermal reduction. **Figure 3i** and **Figure 3j** show the HR–TEM images of Ru/V_2O_3-400 and Ru/V_2O_3-500, respectively, having encapsulating layers of V_2O_3 confirming the occurrence of SMSI.

Figure 4a shows the XPS of freshly reduced Ru/V_2O_3 catalysts at different temperatures. For all the catalysts an asymmetric photoemission signal centred at 280.0 eV was observed, which was assigned to Ru 3d 5/2 emission [37], and was fitted with two component peaks. The major component at 280.0 eV was assigned to metallic ruthenium species and the minor component at 280.7 eV was assigned to $Ru^{\delta+}$ species. The presence of $Ru^{\delta+}$ species was attributed to Ru atoms at the interface with V_2O_3 [38]. The percentage of metallic Ru on the surface increased with reduction temperature from 76 % for Ru/V_2O_3-200 °C to 91 % for Ru/V_2O_3-500 °C (**Figure S4**). The increase in metallic component could be ascribed due to increase in reduction temperature, which causes reduction of the interface region to a higher extent. According to literature this reduction of interface leads to charge transfer from support to metal, which causes the SMSI phenomenon [39].

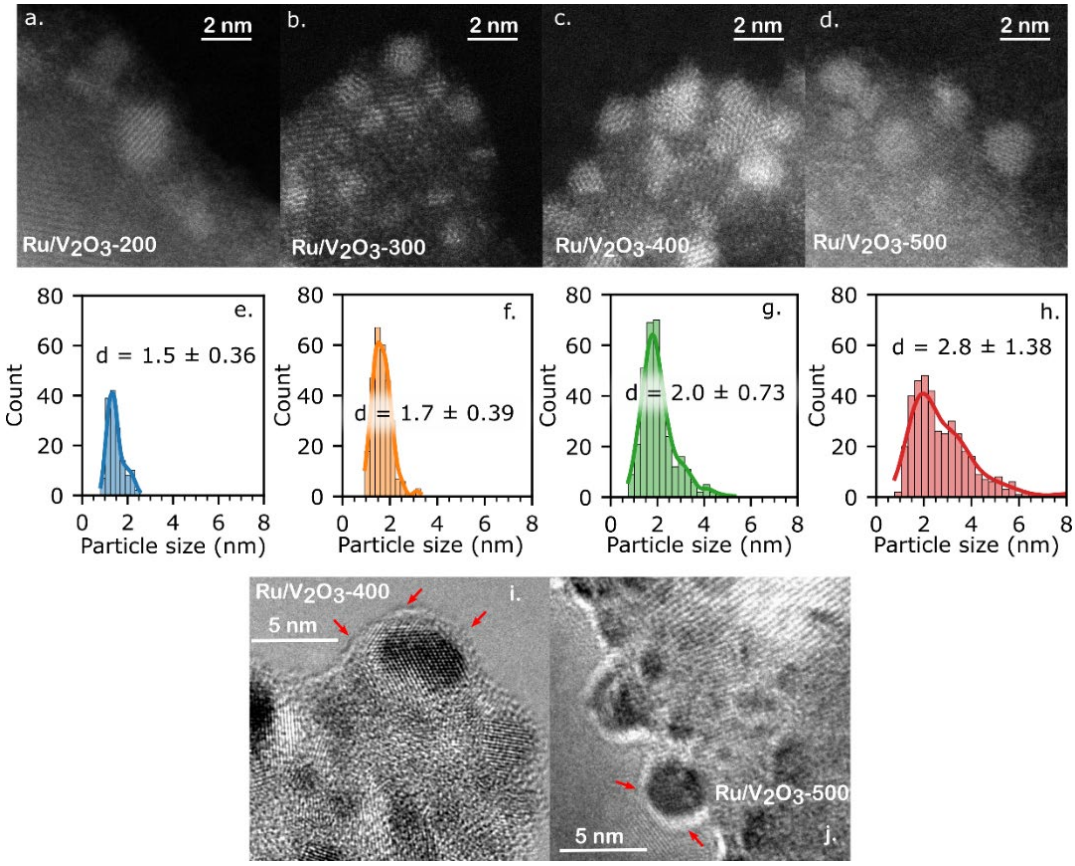

Figure 3.(a-d) STEM images of Ru/V2O3 catalysts reduced at different temperatures. (e-h) Particle size distribution of Ru/V2O3 at different reduction temperatures. (i, j) HR-TEM images of Ru/V2O3-400 and Ru/V2O3-500.

In the O 1s region, two peaks centered at 530.0 eV and 531.6 eV were observed, which were assigned to the lattice oxygen of V_2O_3 and surface hydroxyl groups, respectively. The abundance of surface hydroxyl groups reduced with an increase in reduction temperature because of dehydroxylation of support. This was further confirmed by a decrease in ratio of surface oxygen to vanadium with the increase in reduction temperature (**Figure 4b**). Despite the loss of some surface oxygen species the oxidation state of vanadium was V^{3+} as observed in the V 2p 3/2 region of the spectrum showing a single component peak at 515.6 eV (**Figure 4a**).[40].

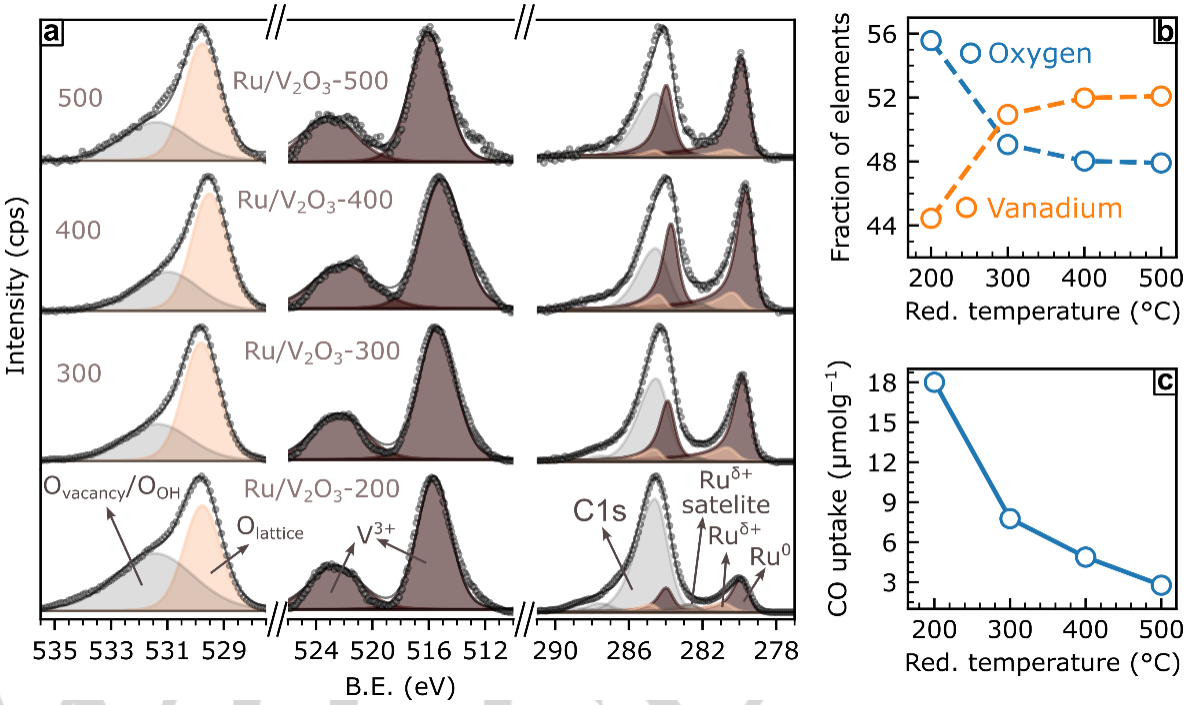

Figure 4.(a) Deconvoluted O 1s, V 2p and Ru 3d 5/2 XPS of Ru/V_2O_3 reduced at different temperatures. (b) Variation of surface elemental composition as a function of reduction temperature. (c) CO chemisorption amount on Ru/V_2O_3 at different reduction temperatures.

Partial reduction of metal support interface is associated with the SMSI effect in supported metal oxides. Partial reduction lowers the work function causing charge transfer from support to metal nanoparticle and encapsulation of the metal nanoparticle [39]. **Figure 4c** shows that CO chemisorption amount decreased with an increase in reduction temperature, which corroborates with loss of chemisorption sites due to encapsulation of Ru nanoparticles by V_2O_3 layer as SMSI progresses.

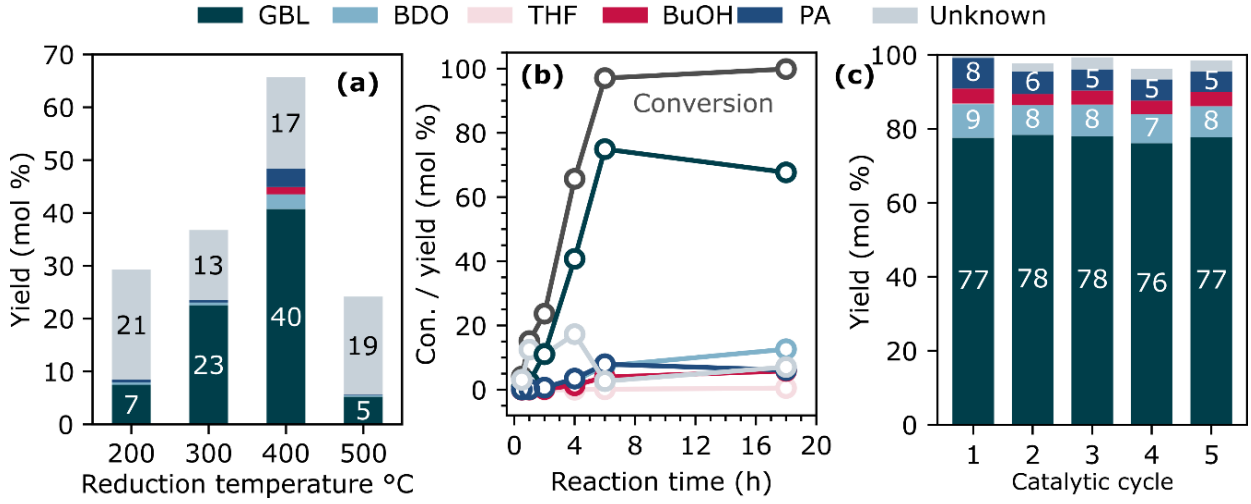

Figure 5. (a) Activity of Ru/V_2O_3 catalysts as a function of reduction temperature, reaction conditions – succinic acid 0.118 g (1 mmol), catalyst 0.05 g, water 5 mL, H_2 5 MPa, 150 °C, 4 h. (b) Succinic acid hydrogen reaction time course, reaction conditions – succinic acid 0.118 g (1 mmol), catalyst Ru/V_2O_3-400 (0.05g), H_2 5 MPa, 150 °C. (c) Catalyst recycling study of Ru/V_2O_3-400 at full conversion, reaction conditions – succinic acid 0.118 g (1 mmol), catalyst 0.05 g, H_2 5 MPa, 150 °C, 6 h. Unknown in the figures represents difference between succinic acid conversion and total yield of detected products, total height of the bars in bar plots represent total conversion.

Succinic acid hydrogenation

Figure 5a shows the result of succinic acid hydrogenation at 150 °C in water in the presence of Ru/V_2O_3 catalysts as a function of the reduction temperature. In all cases, GBL was the major product with small amounts of BDO, THF, butanol (BuOH), and propionic acid (PA). Possible reaction pathways for all these products are shown in **Figure S5**. Direct hydrogenation of one of the carboxylic acid groups of succinic acid, followed by a spontaneous cyclization would lead to the formation of GBL. The yield of GBL increased with an increase in reduction temperature up to 400 °C. Further increase in the reduction temperature to 500 °C decreased the catalytic activity for succinic acid hydrogenation. The evolution of products over time was studied to understand the optimal reaction time using Ru/V_2O_3-400 catalyst (**Figure 5b**). Succinic acid conversion reached 97 % in 6 hours and GBL yield was 77 %. The Ru/V_2O_3-400 catalyst was found to be recyclable for at least up to 5 cycles and there was no loss of activity (**Figure 5c**). The XRD analysis of the used catalyst showed V_2O_3 crystal structure was intact with emergence of a small peak for the VO_2 phase (**Figure S6**). However, since there is no loss of activity over five cycles, this phase change is likely occurring in V_2O_3 regions that are away from the catalytic active center and do not influence the hydrogenation of succinic acid.

Role of SMSI in minimization of substrate induced poisoning on hydrogen dissociation.

The results of succinic acid hydrogenation, with the catalyst reduced at 400 °C, at different hydrogen pressures are shown **Figure S7**. There is a gradual increase in activity with an increase in hydrogen pressure, which suggests that hydrogen dissociation is important in the reaction. As the catalyst reduced at 200 °C showed low activity for succinic acid hydrogenation even though it contained the highest number of exposed Ru particles as per CO chemisorption, SMSI might have a role to play in hydrogen dissociation. Furthermore, the apparent activation energy for Ru/V_2O_3-400 was determined to be 32 kJ mol^{-1}, **(Figure S8)** which as lower than the reported value for Ru/Al_2O_3 (78.9 kJ mol^{-1}) [3], suggesting a distinct reaction mechanism facilitated by SMSI. To investigate the role of SMSI on catalytic activity we studied the hydrogen dissociation over the catalyst by H_2-D_2 exchange in the presence and absence of an adsorbate.

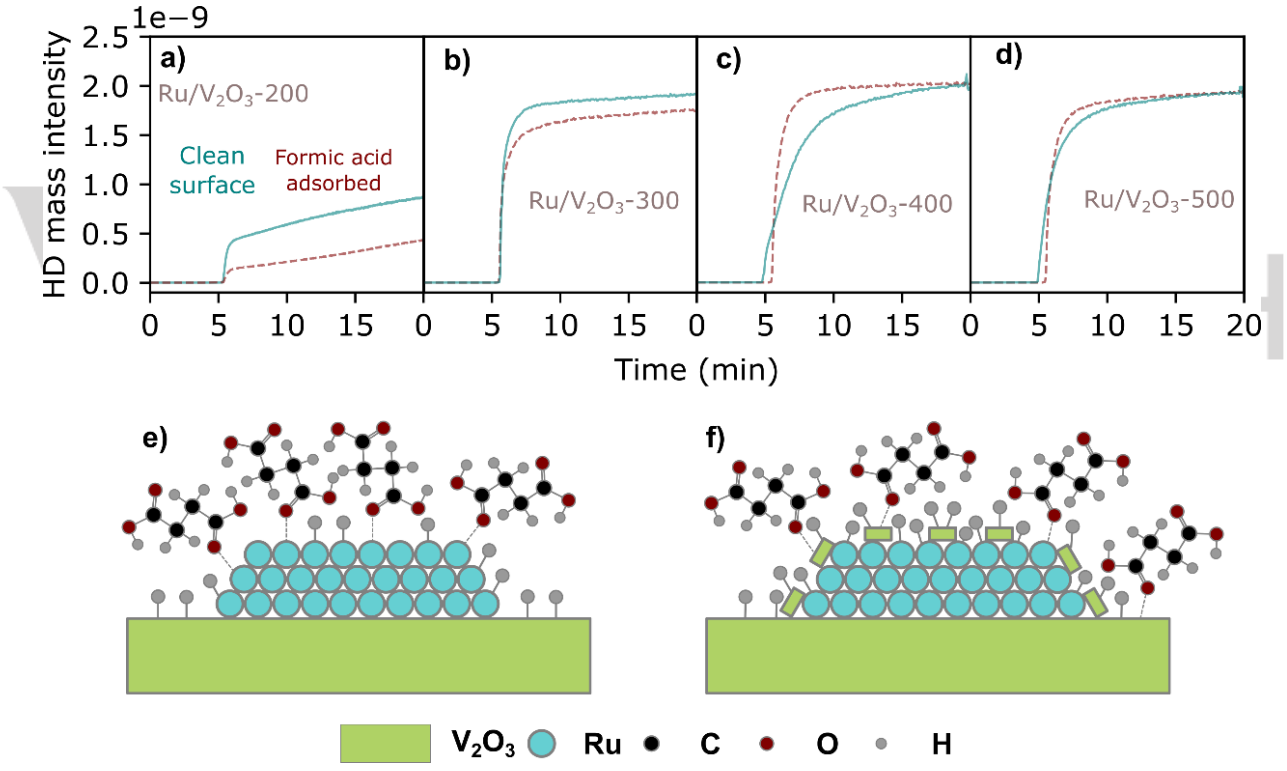

Figure 6. (a-d) Mass intensity of HD in the presence of Ru/V_2O_3 catalysts in the absence and presence of formic acid on the surface. (e, f) Schematic representation of the effect of formic acid adsorption on the catalysts with and without SMSI.

A mixture of H_2-D_2 was flowed over a freshly reduced catalyst while measuring the HD intensity. The H-D exchange reaction was allowed to reach a steady state at 50 °C. All catalysts except Ru/V_2O_3-200 showed similar HD intensity in the absence of any adsorbate (denoted as clean surface in **Figure 6 a-d**). Because the degree of SMSI was higher as temperature increased, we propose that hydrogen spillover at the interface of Ru and V_2O_3, formed via SMSI, contributed towards the higher rate of H-D exchange.

Next, we adsorbed formic acid on the catalysts to test the H-D exchange ability in the presence of an adsorbate with a carboxyl group. Formic acid was chosen over succinic acid as an adsorbate because formic acid is volatile and can be deposited over the catalyst in situ after reduction. The HD intensity over Ru/V_2O_3-200 decreased further in the presence of formic acid, indicating that Ru surface without a suitable extent of SMSI was poisoned by the adsorbate and the hydrogen dissociation ability reduced. However, with the increase in catalyst reduction temperature, the HD intensity for Ru/V_2O_3-400 in the presence of formic acid was similar to the HD intensity over clean surface. These results suggest that coverage of Ru surface by V_2O_3 mitigates the poisoning of the

catalyst. In the catalyst with a higher extent of SMSI the formic acid would adsorb over the V_2O_3 layer instead of Ru sites and would prevent the loss of hydrogen dissociation ability (**Figure 6 e-f**).

Hydrogen dissociation and spillover over interface of Ru/V_2O_3

Through the HD exchange experiment, it was evident that SMSI enhanced the H_2 dissociation ability in the presence of an adsorbate. In the catalyst with SMSI, hydrogenation of succinic acid adsorbed on the V_2O_3 layer would require spillover of H_2. The spillover was studied by analyzing the reduction of WO_3 in a physical mixture of Ru/V_2O_3 and WO_3. First, temperature programmed reduction (TPR) of Ru/V_2O_3 (**Figure 7a**) was measured, which showed a broad reduction peak between 300 °C and 480 °C. In comparison, the TPR profile of Ru/SiO_2 (prepared as a control catalyst) was narrower and spanned from 200 °C to 300 °C, suggesting a stronger interaction between Ru and V_2O_3 compared to that of Ru and SiO_2. The larger area and the asymmetric shape of the reduction peak in case of Ru/V_2O_3 suggest partial reduction of V_2O_3 support. Partial reduction of support is known to trigger the diffusion of support phase onto the metal nanoparticle in case of reducible oxides to cause SMSI [39]

TPR profile of physical mixture of tungsten oxide and Ru/SiO_2 was similar to pure Ru/SiO_2 with a rising tail around 600 °C. The reduction of physically mixed tungsten oxide would require the spillover of dissociated hydrogen to reduce WO_3 as shown in **Figure 7c**. When the TPR experiment was conducted with a physical mixture of WO_3 and Ru/V_2O_3 a new peak centered around 500 °C appeared, which was assigned to reduction of WO_3 via spillover of dissociated hydrogen. XPS of the physical mixture after the TPR experiment showed the presence of significant amount of W^{5+} (**Figure 7b**), which confirmed the ease of hydrogen spillover over V_2O_3.

.

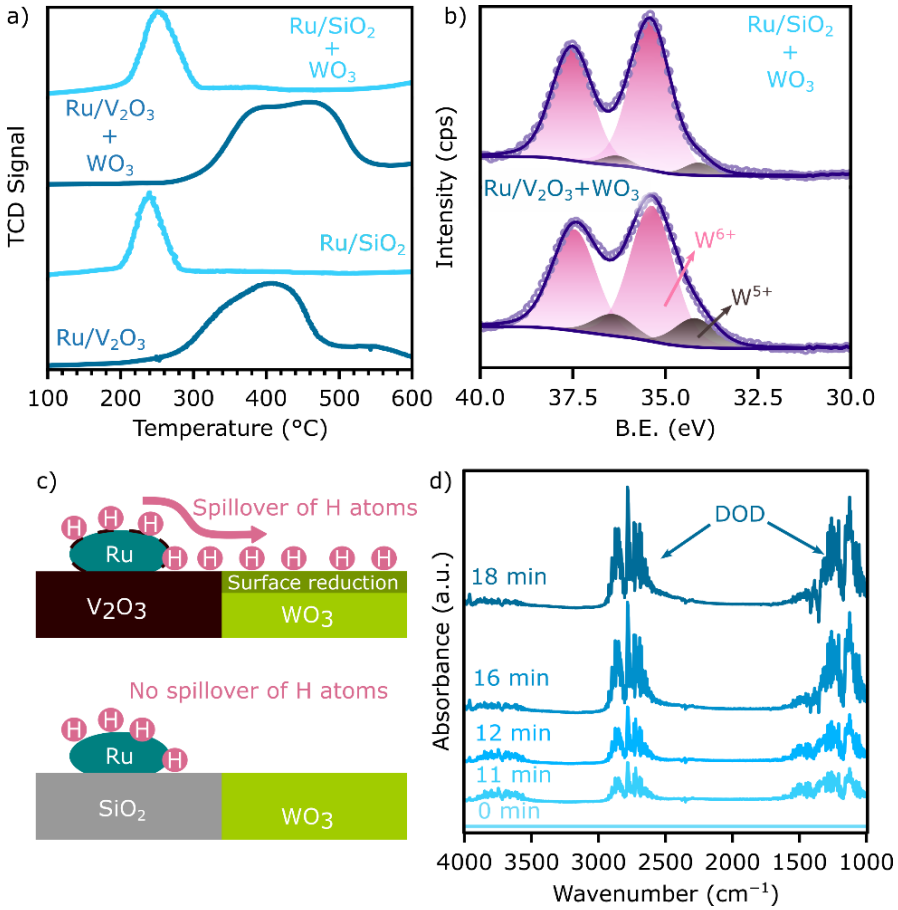

Figure 7. (a) TPR profiles of Ru/V_2O_3 and Ru/SiO_2 and their physical mixture with WO_2. (b) W 4f XPS of physical mixtures of Ru/V_2O_3 and Ru/SiO_2 with WO_3 after the TPR experiment. (c) Scheme showing surface reduction of WO_3 in physical contact with Ru/V_2O_3 due to hydrogen spillover. (d) In situ D_2 FTIR over Ru/V_2O_3 400 catalyst.

Hydrogen spillover involves either the migration of a hydrogen atom or a proton from the metal to support. While the electrons would enter the conduction band of the support, the protons would bond to the surface oxygen species. In the absence of reactants, the formed OH groups would eventually lead to the formation of either surface or gas phase water molecules, which was monitored by in situ IR spectroscopy. When D_2 was flowed through the sample reduced in situ at 400 °C, there was a gradual increase in signal around 2500 to 3000 cm^{-1} region and 1300 to 1000 cm^{-1} as shown in **Figure 7d**. The former was attributed to OD stretching frequency and the latter to OD bending frequency [44–46]. The OD formation on oxide supports could also occur via exchange of D with support hydroxyl protons. However, loss of hydroxyl protons in such a manner must be accompanied by the development of negative peak around OH region in the IR spectrum, which was not observed. Hence, the formation of OD could be assigned to the spilled over D^+ ions indicating formation of a proton-hydride pair and spillover mechanism for Ru/V_2O_3 catalysts with SMSI.

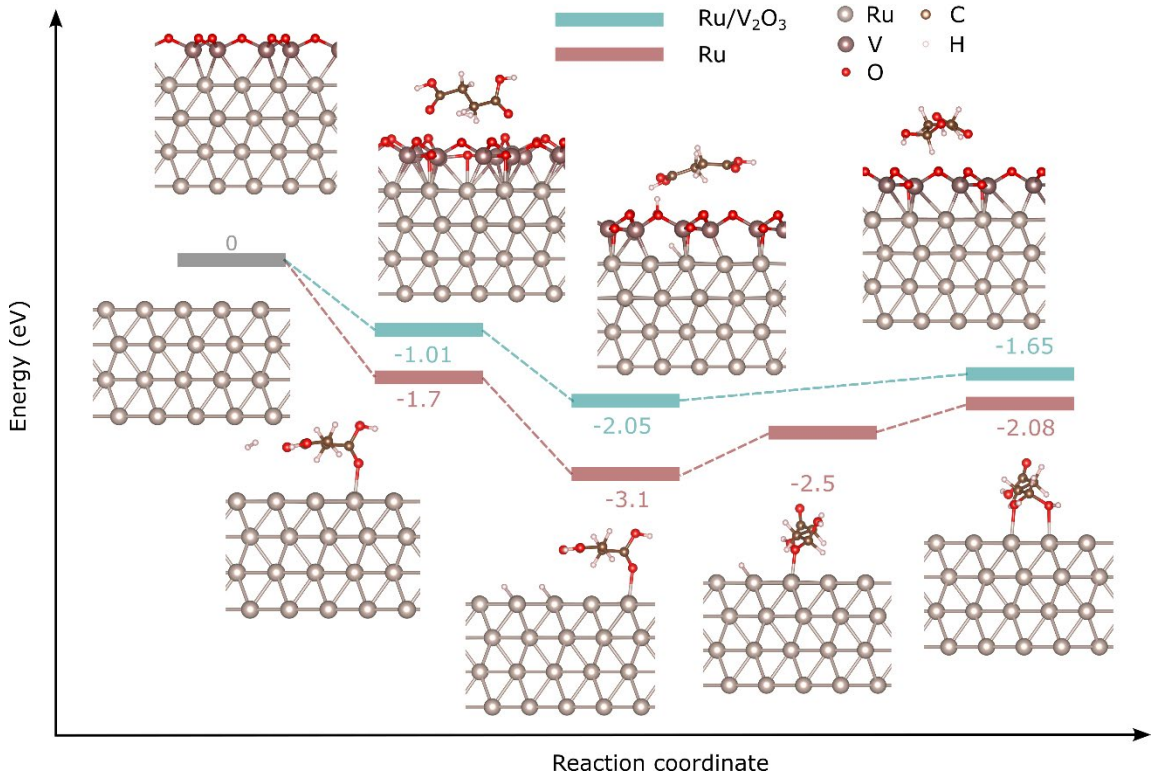

Figure 8. Reaction free energy (ΔG in eV) profile of various intermediates in the succinic acid hydrogenation over bare ruthenium surface and Ru/V_2O_3 surface.

DFT calculation to show hydrogen heterolysis is more efficient in succinic acid hydrogenation

Experimental observations of SMSI and its effect in enhancing hydrogenation of succinic acid were also evaluated by theoretical calculations. The Ru/V_2O_3 catalyst with SMSI was modelled considering a monolayer of V_2O_3 deposited on Ru (001) and it was compared with bare Ru (001) as a model for catalyst without SMSI (**Figure 8**, and **Figure S9-S10**). Calculation results showed that homolytic dissociation of H_2 was preferred over bare Ru (001) surface (Int 2, **Figure S9**). In contrast, H_2 underwent heterolytic cleavage on the Ru/V_2O_3 surface where V_2O_3 monolayer is present on the surface exposing Ru surface partially (Int 2, **Figure S10**). The heterolytic cleavage on Ru/V_2O_3 was possible due to the presence of electron rich O of V_2O_3 layer and the partially exposed electron deficient Ru, which attracted the proton and the hydride, respectively. Upon introduction of succinic acid, a sequential hydrogenation pathway was observed on the bare Ru (001). Consecutive transfer of dissociated H occurred from the bare Ru (001) surface to the carbonyl carbon and oxygen atom of succinic acid. The overall change in reaction free energy (**Figure 8**) for the consecutive steps was 1.02 eV (-3.10 eV to -2.08 eV). However, for Ru/V_2O_3, hydrogenation with proton and hydride in a concerted mechanism was more favored. The change in reaction free energy was 0.40 eV (-2.05 eV to -1.65 eV), which was less than that for bare Ru(001) without SMSI. In addition, the desorption of the product from the Ru/V_2O_3 surface was more favored with a desorption energy of 0.83 eV. Whereas the desorption of product from bare Ru(001) surface requires much higher energy of 1.53 eV. Therefore, the calculation results show that succinic acid hydrogenation through heterolytic dissociation of H_2, desorption of product and regeneration of the active site would be facile on the Ru/V_2O_3 catalyst surface with SMSI, which aligns with the experimental outcomes

Conclusion

In conclusion, the SMSI effect, along with hydrogen spillover in Ru/V_2O_3 could lead to effective hydrogenation of succinic acid at mild condition by reducing substrate induced poisoning of hydrogen dissociation sites. STEM and TEM images along with XPS and CO pulse chemisorption confirmed the occurrence of SMSI effect in Ru/V_2O_3 catalysts reduced at higher temperature. The catalyst reduced at 400 °C with optimal SMSI degree produced a GBL yield of 77 % at mild condition of 150 °C and in the presence of water. A decrease in HD formation from H_2–D_2 exchange reaction in presence of adsorbed formic acid illustrated poisoning of hydrogen dissociation sites in catalysts without SMSI. In situ D_2 IR confirmed formation of proton-hydride species on V_2O_3 surface owing to heterolytic dissociation. According to density functional theory calculations, easier hydrogenation and facile desorption of product from the Ru/V_2O_3 surface in SMSI state make it a better catalyst for the process compared to clean Ru surface. The enhanced activity at mild conditions along with improved stability due to SMSI enables economical and long-term operation in an industrial setting. Moreover, the ability to operate under aqueous conditions enhances its feasibility for industrial applications.

Supporting Information

Supporting information contains additional experimental details, figures and tables. The authors have cited additional references within the Supporting Information.[47,48]

Acknowledgements

Part of this research was supported by the JACI Prize for Encouraging Young Researcher and Hokkaido University Creative Young Researcher Acceleration Project. A part of this work was supported by "Advanced Research Infrastructure for Materials and Nanotechnology in Japan (ARIM)" of the Ministry of Education, Culture, Sports, Science and Technology (MEXT), proposal number JPMXP1223HK0088 and JPMXP1224HK0068. Also, we thank IIT Indore for the computing facilities. Part of this work is supported by DST-SERB (Project Number CRG/2022/000836), CSIR (Project Number 01(3046)/21/EMR-II). E.M. thanks MoE for research fellowship.

Keywords: strong metal support interaction •V_2O_3 support • succinic acid hydrogenation • hydrogen spillover • catalyst poisoning

[1] G. Budroni, A. Corma, *J. Catal.* **2008**, *257*, 403–408.
[2] U. G. Hong, S. Hwang, J. G. Seo, J. Lee, I. K. Song, *J. Ind. Eng. Chem.* **2011**, *17*, 316–320.
[3] K. Yakabi, A. Jones, A. Buchard, A. Roldan, C. Hammond, *ACS Sustain. Chem. Eng.* **2018**, *6*, 16341–16351.
[4] C. Zhang, L. Chen, H. Cheng, X. Zhu, Z. Qi, *Catal. Today* **2016**, *276*, 55–61.
[5] C. You, C. Zhang, L. Chen, Zhiwen. Qi, *Appl. Organomet. Chem.* **2015**, *29*, 653–660.
[6] B. Tapin, F. Epron, C. Especel, B. K. Ly, C. Pinel, M. Besson, *ACS Catal.* **2013**, *3*, 2327–2335.
[7] D. P. Minh, M. Besson, C. Pinel, P. Fuertes, C. Petitjean, *Top. Catal.* **2010**, *53*, 1270–1273.
[8] K. H. Kang, U. G. Hong, Y. Bang, J. H. Choi, J. K. Kim, J. K. Lee, S. J. Han, I. K. Song, *Appl. Catal. Gen.* **2015**, *490*, 153–162.
[9] S. D. Le, S. Nishimura, *Appl. Catal. B Environ.* **2021**, *282*, 119619.
[10] Z. Shao, C. Li, X. Di, Z. Xiao, Changhai. Liang, *Ind. Eng. Chem. Res.* **2014**, *53*, 9638–9645.
[11] X. Di, C. Li, B. Zhang, J. Qi, W. Li, D. Su, C. Liang, *Ind. Eng. Chem. Res.* **2017**, *56*, 4672–4683.
[12] R. M. Deshpande, V. V. Buwa, C. V. Rode, R. V. Chaudhari, P. L. Mills, *Catal. Commun.* **2002**, *3*, 269–274.
[13] X. Liu, X. Wang, G. Xu, Q. Liu, X. Mu, Haichao. Liu, *J. Mater. Chem. Mater. Energy Sustain.* **2015**, *3*, 23560–23569.
[14] S. Oka, *Bull. Chem. Soc. Jpn.* **1962**, *35*, 986–989.
[15] H. Kim, S. Yang, D. H. Kim, *Environ. Res.* **2020**, *187*, 109667.
[16] L. Wang, H. Guo, Q. Xie, J. Wang, B. Hou, L. Jia, J. Cui, D. Li, *Appl. Catal. Gen.* **2019**, *572*, 51–60.
[17] J. H. Ter Horst, R. M. Geertman, G. M. Van Rosmalen, *J. Cryst. Growth* **2001**, *230*, 277–284.
[18] W. Schwarz, J. Schossig, R. Rossbacher, R. Pinkos, H. Höke, in *Ullmanns Encycl. Ind. Chem.*, Wiley-VCH, Weinheim, **2019**, pp. 1–7.
[19] L. Karam, C. N. Neumann, *ChemCatChem* **2022**, *14*, e202200953.
[20] Y. Takeda, M. Tamura, Y. Nakagawa, K. Okumura, K. Tomishige, *ACS Catal.* **2015**, *5*, 7034–7047.
[21] M. Guo, X. Kong, C. Li, Q. Yang, *Commun. Chem.* **2021**, *4*, 1–10.
[22] X. Cui, Y. Li, C. Topf, K. Junge, M. Beller, *Angew. Chem. Int. Ed.* **2015**, *54*, 10596–10599.
[23] A. Primo, P. Concepción, A. Corma, *Chem. Commun.* **2011**, *47*, 3613–3615.
[24] S. J. Tauster, S. C. Fung, R. T. K. Baker, J. A. Horsley, *Science* **1981**, *211*, 1121–1125.
[25] S. J. Tauster, S. C. Fung, R. L. Garten, *J. Am. Chem. Soc.* **1978**, *100*, 170–175.
[26] S. J. Tauster, S. C. Fung, *J. Catal.* **1978**, *55*, 29–35.
[27] G. Kresse, J. Furthmüller, *Phys. Rev. B* **1996**, *54*, 11169.
[28] G. Kresse, J. Hafner, *Phys. Rev. B* **1993**, *47*, 558.
[29] P. E. Blöchl, *Phys. Rev. B* **1994**, *50*, 17953–17979.
[30] G. Kresse, D. Joubert, *Phys. Rev. B* **1999**, *59*, 1758–1775.
[31] J. P. Perdew, K. Burke, M. Ernzerhof, *Phys. Rev. Lett.* **1996**, *77*, 3865–3868.
[32] S. Grimme, J. Antony, S. Ehrlich, H. Krieg, *J. Chem. Phys.* **2010**, *132*, 154104.
[33] V. I. Anisimov, F. Aryasetiawan, A. I. Lichtenstein, *J. Phys. Condens. Matter* **1997**, *9*, 767.
[34] S. L. Dudarev, G. A. Botton, S. Y. Savrasov, C. J. Humphreys, A. P. Sutton, *Phys. Rev. B* **1998**, *57*, 1505–1509.
[35] J. Goniakowski, C. Noguera, *J. Phys. Chem. C* **2019**, *123*, 9272–9281.
[36] G. Kresse, S. Surnev, J. Schoiswohl, F. P. Netzer, *Surf. Sci.* **2004**, *555*, 118–134.
[37] D. J. Morgan, *Surf. Interface Anal.* **2015**, *47*, 1072–1079.
[38] J. Zhou, Z. Gao, G. Xiang, T. Zhai, Z. Liu, W. Zhao, X. Liang, L. Wang, *Nat. Commun.* **2022**, *13*, 327.
[39] Q. Fu, T. Wagner, S. Olliges, H.-D. Carstanjen, *J. Phys. Chem. B* **2005**, *109*, 944–951.
[40] G. Silversmit, D. Depla, H. Poelman, G. B. Marin, R. De Gryse, *J. Electron Spectrosc. Relat. Phenom.* **2004**, *135*, 167–175.
[41] D. A. Panayotov, S. P. Burrows, J. T. Jr. Yates, J. R. Morris, *J. Phys. Chem. C* **2011**, *115*, 22400–22408.
[42] A. Mahdavi-Shakib, L. C. Rich, T. N. Whittaker, B. D. Chandler, *ACS Catal.* **2021**, *11*, 15194–15202.
[43] P. A. Kots, T. Xie, B. C. Vance, C. M. Quinn, M. D. de Mello, J. A. Boscoboinik, C. Wang, P. Kumar, E. A. Stach, N. S. Marinkovic, L. Ma, S. N. Ehrlich, D. G. Vlachos, *Nat. Commun.* **2022**, *13*, 5186.
[44] H. Liu, Y. Wang, J. M. Bowman, *J. Phys. Chem. B* **2016**, *120*, 2824–2828.
[45] H. Belhadj, A. Hakki, P. K. J. Robertson, D. W. Bahnemann, *Phys. Chem. Chem. Phys.* **2015**, *17*, 22940–22946.
[46] R. Stach, P. Krebs, F. Jones, B. Mizaikoff, *CrystEngComm* **2017**, *19*, 14–17.
[47] S. Brunauer, P. H. Emmett, E. Teller, *J. Am. Chem. Soc.* **1938**, *60*, 309–319.
[48] G. Bergeret, P. Gallezot, in *Handb. Heterog. Catal.* (Eds.: G. Ertl, H. Knözinger, F. Schüth, J. Weitkamp), Wiley, **2008**, pp. 738–765.

Entry for the Table of Contents

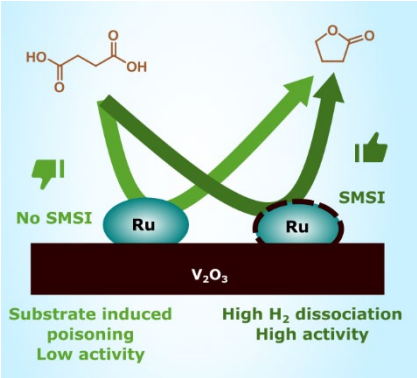

Strong metal support interaction in Ru/V_2O_3 prevents support induced catalyst poisoning in succinic acid hydrogenation reaction leading to higher activity. Strong binding of carboxylic acids to the metal nanoparticles hinders hydrogen dissociation. However, covering the metal nanoparticles by via strong metal support interaction, not only leads to physical separation of carboxylic acids and the metal nanoparticles, but also provides alternative hydrogen dissociation and hydrogenation pathways to boost activity.

Institute and/or researcher Twitter usernames: @YayatiNaresh @Abhijit_Shrotri @ICAT_Hokudai